Supplementary material

for

Structural and dynamic effects of pseudouridine modifications on non-canonical interactions in RNA structures

Jennifer Vögele[1], Elke Duchardt-Ferner[1], Holger Kruse[2], Zhengyue Zhang[2,3,4], Jiri Sponer[2], Miroslav Krepl[2*], Jens Wöhnert[1*]

[1]Institute of Molecular Biosciences and Center for Biomolecular Magnetic Resonance (BMRZ), Goethe-University Frankfurt, Max-von-Laue-Str. 9, 60438 Frankfurt, Germany

[2]Institute of Biophysics of the Czech Academy of Sciences, Kralovopolska 135, 612 65 Brno, Czech Republic

[3]CEITEC−Central European Institute of Technology, Masaryk University, Kamenice 5, 625 00 Brno, Czech Republic

[4]National Centre for Biomolecular Research, Faculty of Science, Masaryk University, Kamenice 5, 625 00 Brno, Czech Republic

Supplementary Text:

QM/MM calculations

Non-periodic QM/MM optimizations using an additive scheme with electrostatic (point-charge) embedding were performed using an in-house modified version of the QM/MM function (Götz et al. 2014) within the sander module of AMBER 18 to enable calculations with Turbomole (Ahlrichs et al. 1989). The initial structures for the QM/MM calculations were taken from carefully selected MD simulation snapshots of each variant of the NSR system. Only snapshots with the structurally essential K^+ ion bound near U14(O4) or Ψ14(O2) were considered (Krepl et al. 2018). The structures were then solvated in a droplet of SPC/E water molecules with a radius of 45 Å. To obtain net-neutral conditions, we added a sufficient number of K^+ ions with a minimal distance of 7 Å between the newly added ions and the NSR. The water droplet was then equilibrated following a previously developed protocol (Pokorná et al. 2018). No cut off for the non-bonded interactions was used. The QM region was defined to contain the area of interest – the U14(N3)/A17(OP2) HB1-bond and other parts of the U-turn, along with a sufficiently sized buffer region (see (Krepl et al. 2018) for details). The boundary region was chosen to preserve the bond polarity at the link H-atom. Technical implementation details can be found in (Götz et al. 2014). In addition to RNA atoms, all solvent molecules within a radius of 5 Å around U14/Ψ14 were included in the QM region. We have used the hybrid-functional based PBEh-3c composite method (Grimme et al. 2015) to describe the QM region, an approach well tested for chemistry in general (Brandenburg et al. 2014) and benchmarked by us for QM/MM optimizations of RNA-protein systems (Pokorná et al. 2018).

Our QM/MM calculations of the individual systems indicated the same trends as observed in the MD simulations. Namely, the stabilizing effect of the U18Ψ replacement was also observed in QM/MM calculations, including shorter HB1 distance with greater stretch of the H3-N3 covalent bond (Supporting Information Table 1) compared to the WT. The Ψ18 is not directly involved in the HB1 interaction, suggesting either an indirect allosteric structural effect of the Ψ18 substitution or electronic structure changes in the A17 phosphate group induced by the PSU18(N1)–A17(O5′) H-bond which favor the HB1 interaction. On the other hand, our QM/MM optimizations of U14Ψ structures, started from two different simulation

snapshots with a well-formed HB1 interaction, revealed a divergent result (Supporting Information Table 1). This reflects insufficient sampling of the QM/MM optimizations and we therefore refrained from making strong conclusions based on these calculations. In case of this study, we suggest the MD results presented in the main text provide a superior computational description of the differences between uridine and pseudouridine NSR variants.

Supplementary Figures:

Supplementary Figure S1.

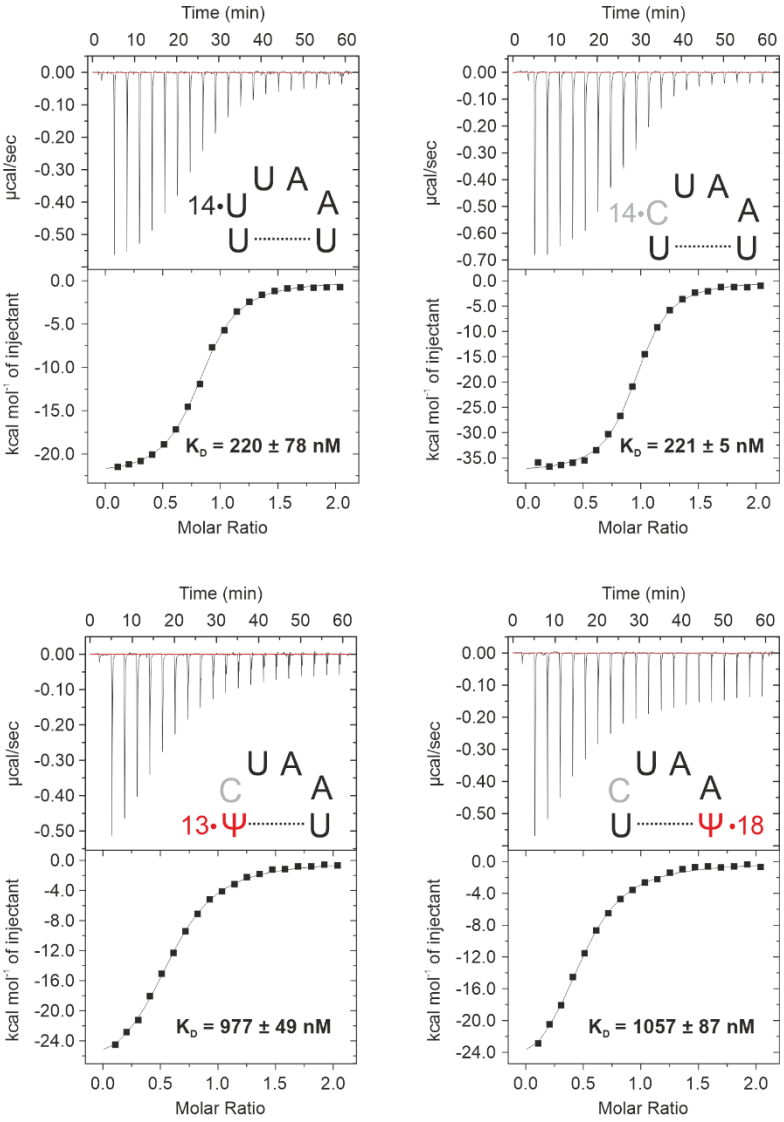

Ribostamycin affinities of the WT NSR (top, left), the U14C NSR (top, right) and the pseudouridine containing variants U14C_U13Ψ (bottom, left) and U14C_U18Ψ (bottom, right). Shown are the respective ITC thermograms (top) and the resulting binding isotherms (bottom). The respective values of the dissociation constants (K_D) which are the averages of three independent experiments are given as insets.

Supplementary Figure S2.

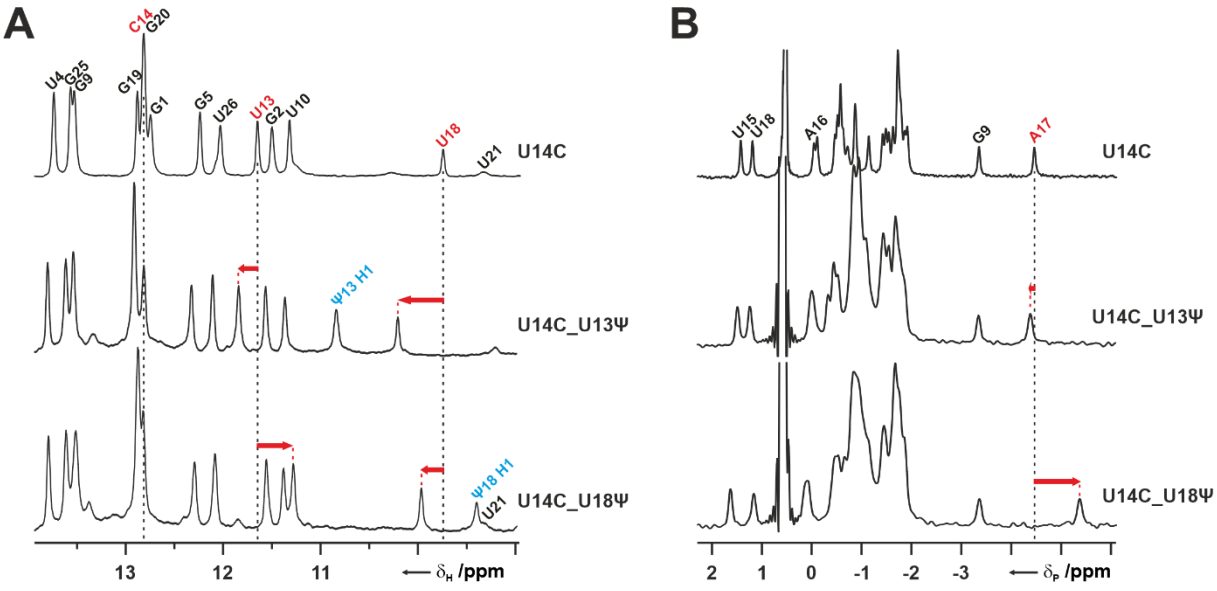

Comparison of the 1D-^{1}H imino proton (A) and the 1D-^{31}P NMR spectra (B) between the unmodified U14C variant of the NSR (top) and the U13Ψ (middle) and the U18Ψ (bottom) modified variants. Significant chemical shift changes caused by the introduction of a pseudouridine nucleotide are marked by red arrows and indicated by vertical dashed lines. Pseudouridine H1 imino proton signals are labeled in blue. H3 imino proton signals of C14+, U13 and U18 and the signal of the A17 phosphate group are labeled in red.

Supplementary Figure S3.

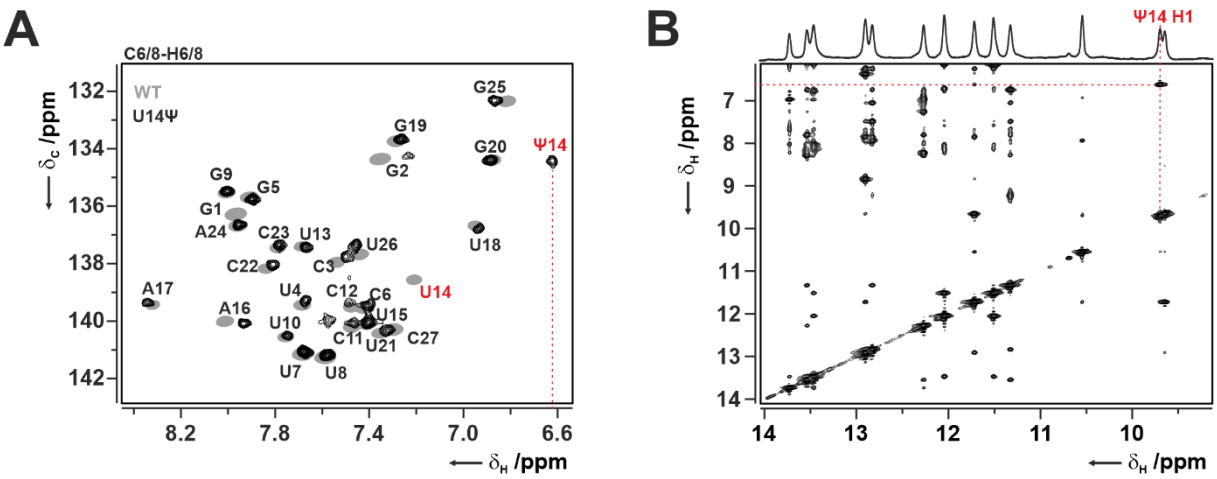

NMR signal assignments for the pseudouridine H6C6 group and the H1 imino proton in the U14Ψ variant of the WT NSR bound to ribostamycin. (A) Overlay of natural abundance $^{1}H,^{13}C$-HSQC-spectra optimized for the aromatic CH groups for the unmodified WT NSR (gray) and the U14Ψ variant (black). The signals for the H6C6 group of U14 and Ψ14, respectively, are labeled in red. (B) Region of a 2D-$^{1}H,^{1}H$-NOESY-spectrum that contains NOEs between imino-protons and between imino and aromatic protons. The signal of the H1 imino proton of the pseudouridine is identified by its strong NOE cross peak to the H6 proton of the same nucleotide.

Supplementary Figure S4.

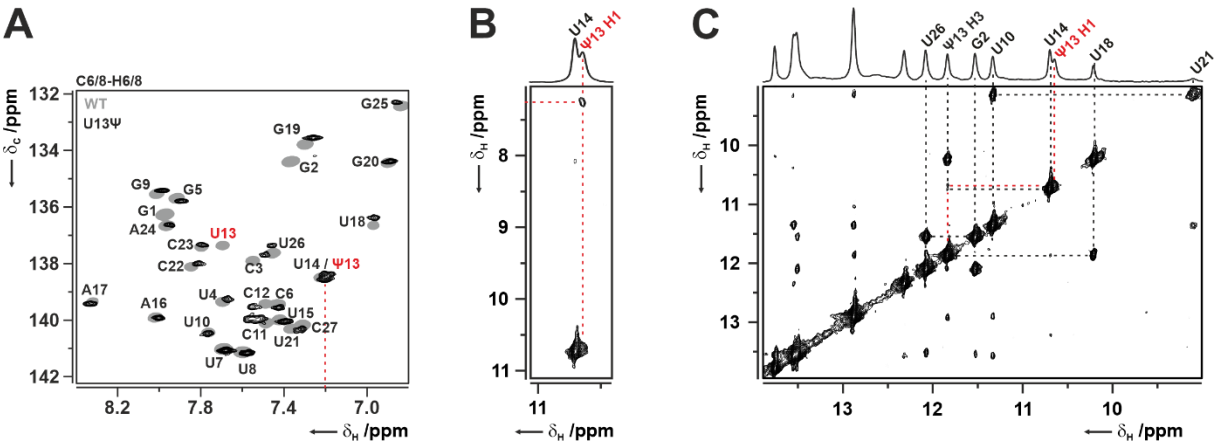

NMR signal assignments for the pseudouridine H6C6 group and the H1 imino proton in the U13Ψ variant of the WT NSR bound to ribostamycin. (A) Overlay of natural abundance $^{1}H,^{13}C$-HSQC-spectra optimized for the aromatic CH groups for the unmodified WT NSR (gray) and the U13Ψ variant (black). The signals for the H6C6 group of U13 and Ψ13, respectively, are labeled in red. (B) Close-up from a 2D-$^{1}H,^{1}H$-NOESY-spectrum that shows the NOE cross peak from the signal of the H1 imino proton of the pseudouridine to the H6 proton of the same nucleotide. (C) Imino proton region of a 2D-$^{1}H,^{1}H$-NOESY-spectrum showing internucleotide cross peaks that enable imino proton signal assignments as indicated by dashed lines.

Supplementary Figure S5.

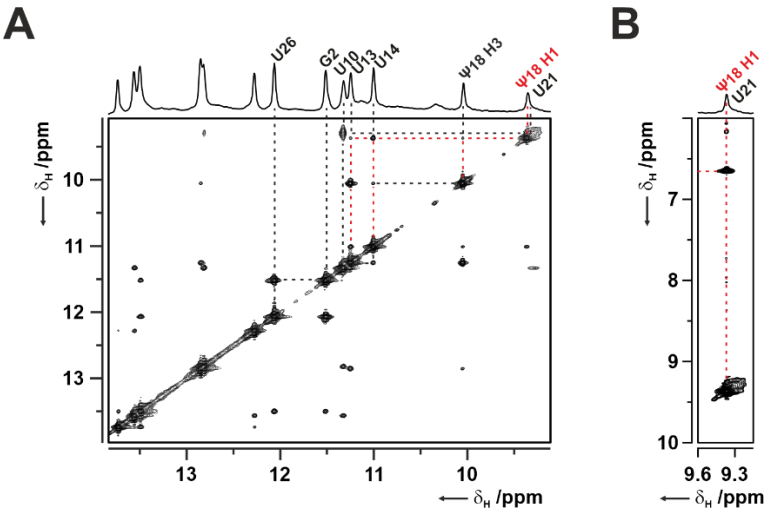

(A) Imino proton region of a 2D-^{1}H,^{1}H-NOESY-spectrum for the U18Ψ variant of the WT NSR showing internucleotide cross peaks that enable imino proton signal assignments as indicated by dashed lines. (B) Close-up from a 2D-^{1}H,^{1}H-NOESY-spectrum that shows the NOE cross peak from the signal of the H1 imino proton of the pseudouridine to the H6 proton of the same nucleotide.

Supplementary Figure S6.

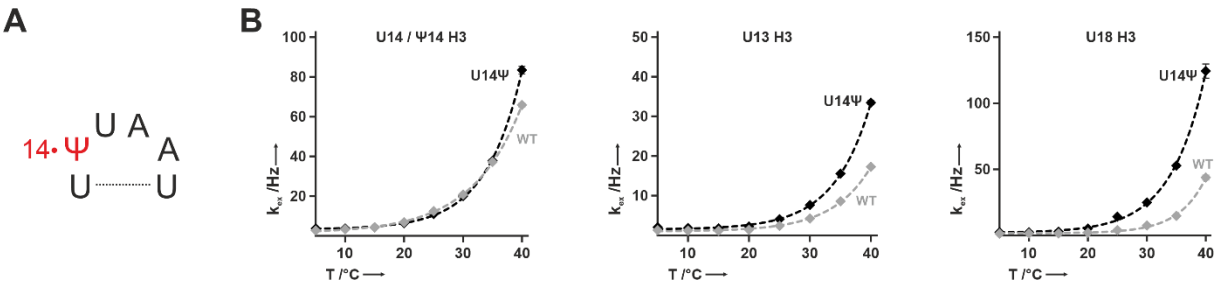

(A) Loop sequence of the U14Ψ variant of the WT NSR. (B) Temperature dependence of the water exchange rates for the H3 imino protons of the Ψ14 (left), U13 (middle) and U18 (right) nucleotides for the U14Ψ variant. For comparison the corresponding curves for the respective H3 imino protons of the unmodified WT NSR are shown in grey in each panel. The broken lines are not the result of curve fitting but only intended to guide the eye.

Supplementary Figure S7.

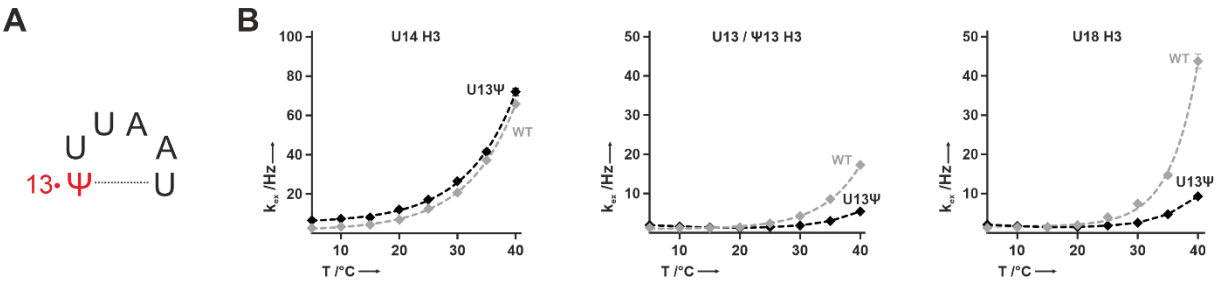

(A) Loop sequence of the U13Ψ variant of the WT NSR. (B) Temperature dependence of the water exchange rates for the H3 imino protons of the U14 (left), Ψ13 (middle) and U18 (right) nucleotides for the U13Ψ variant. For comparison the corresponding curves for the respective H3 imino protons of the unmodified WT NSR are shown in grey in each panel. The broken lines are not the result of curve fitting but only intended to guide the eye.

Supplementary Figure S8.

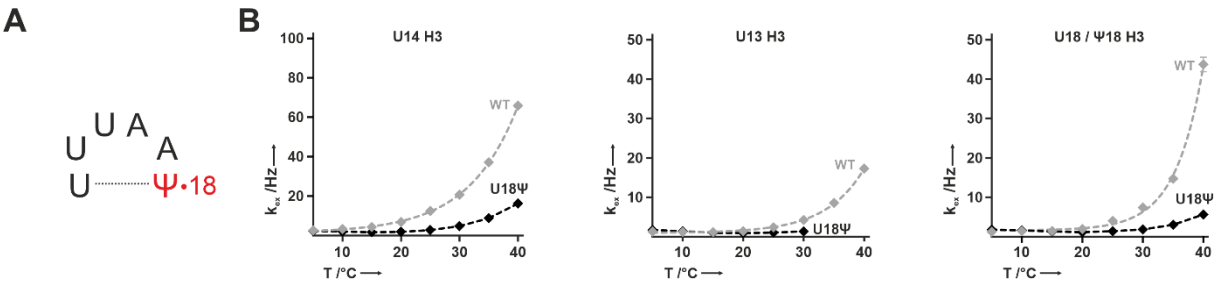

(A) Loop sequence of the U18Ψ variant of the WT NSR. (B) Temperature dependence of the water exchange rates for the H3 imino protons of the U14 (left), U13 (middle) and Ψ18 (right) nucleotides for the U18Ψ variant. For comparison the corresponding curves for the respective H3 imino protons of the unmodified WT NSR are shown in grey in each panel. The broken lines are not the result of curve fitting but only intended to guide the eye.

Supplementary Figure S9.

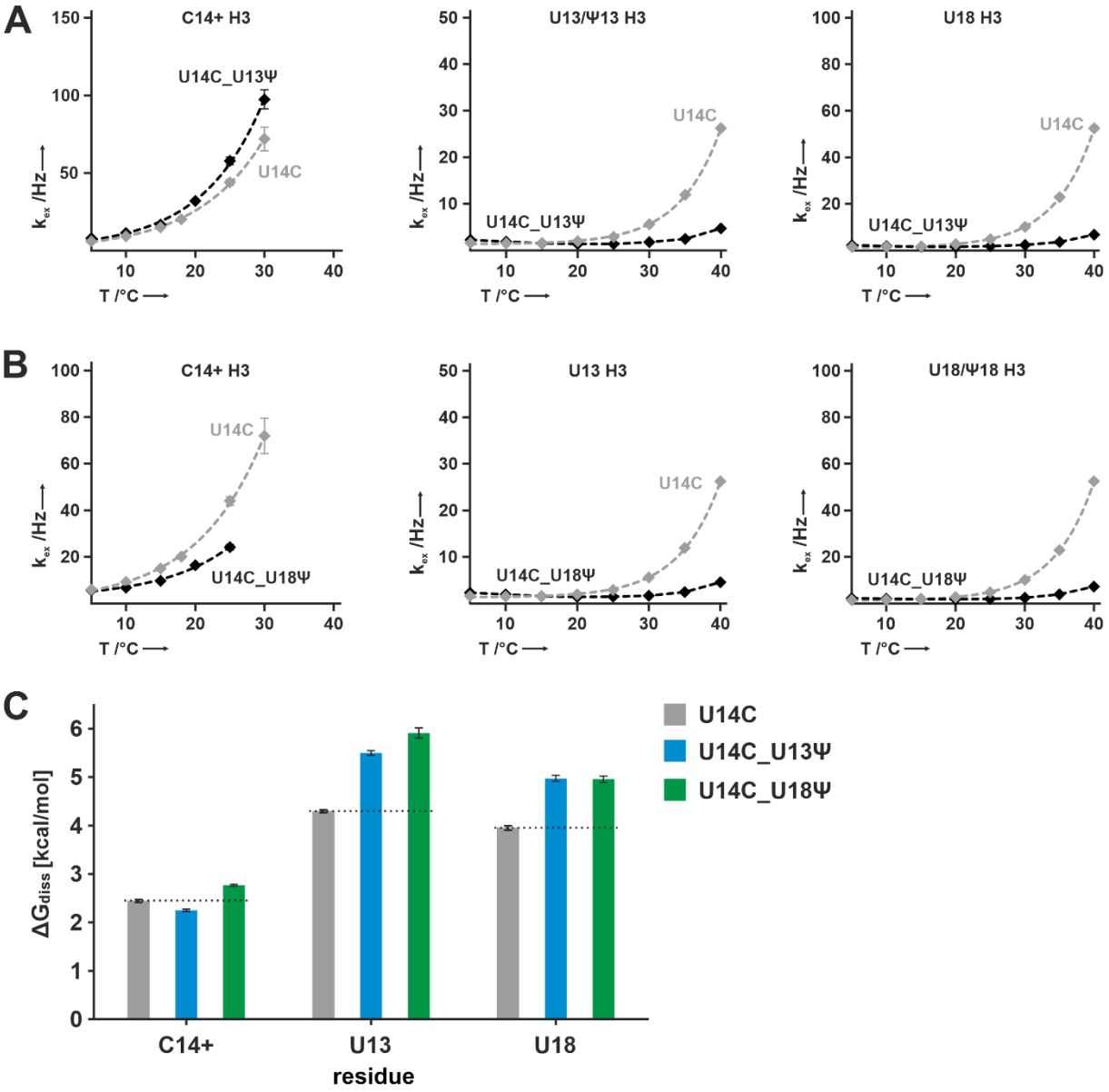

(A) Temperature dependence of the H3 imino proton water exchange rates for the C14+ (left), the Ψ13/U13 (middle) and the U18 (right) imino protons in the U14C_U13Ψ variant (black) in comparison to the unmodified U14C NSR (gray). The signature HB1 interaction is weakened in this variant while the Ψ13:U18 base pair is significantly stabilized compared to the U13:U18 base pair in the unmodified U14C NSR. (B) Temperature dependence of the H3 imino proton water exchange rates for the C14+ (left), the U13 (middle) and the Ψ18/U18 (right) imino protons in the U14C_U18Ψ variant (black) in comparison to the unmodified U14C NSR (gray).

The signature HB1 interaction and the U13:Ψ18 base pair are significantly stabilized compared to the unmodified U14C NSR. (C) Dissociation free energy ΔG_{diss} at T = 25 °C for the signature HB1 interaction (left) and the hydrogen bonds involving the U/Ψ13 H3 and U/Ψ18 H3 protons (middle and right, respectively) in the NSR variants U14C (grey), U14C_U13Ψ (blue) and U14C_U18Ψ (green). The dashed lines correspond to ΔG_{diss} for the interactions in the U14C NSR.

Supplementary Figure S10.

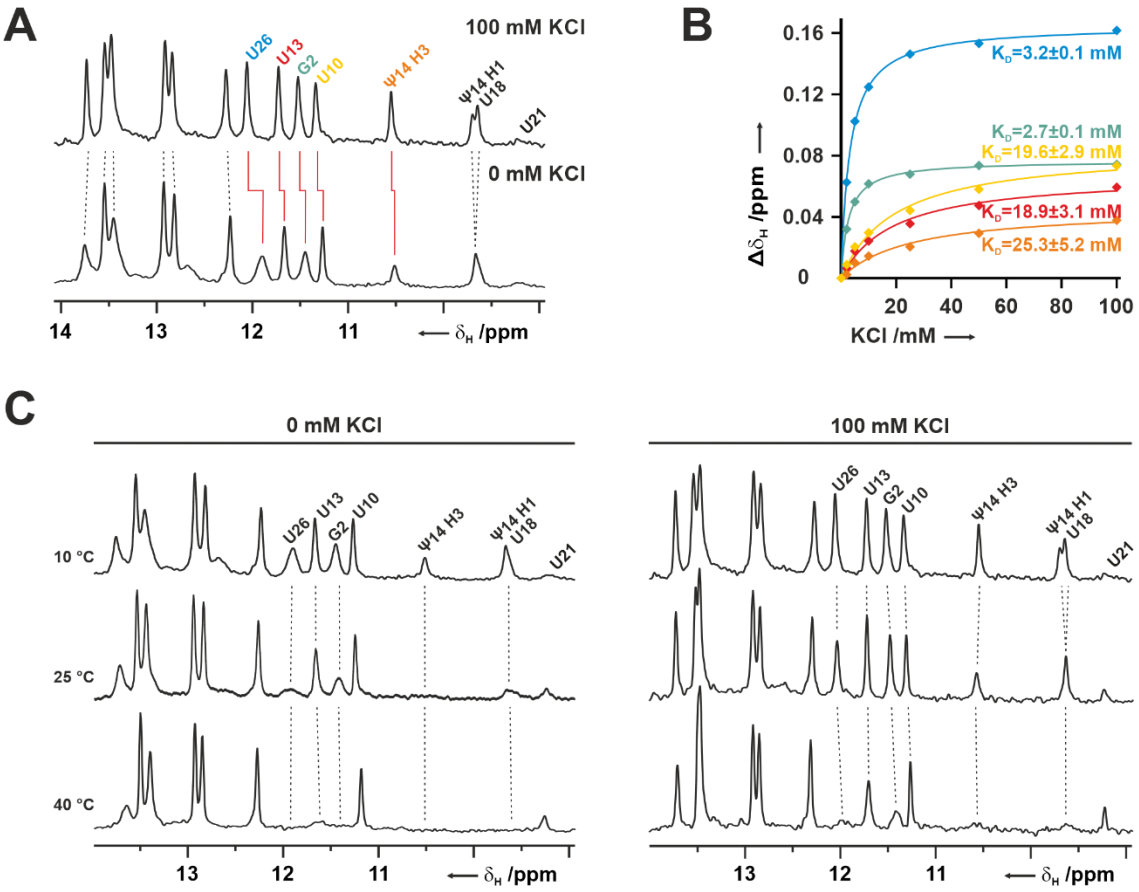

Potassium ion binding to the WT NSR U14Ψ variant. (A) Chemical shift changes of the imino proton resonances induced by the addition of 100 mM potassium chloride to the U14Ψ RNA in 50 mM BisTris buffer. (B) Chemical shift changes as a function of KCl concentration for G2 (light green) and U26 (blue) of the G:U wobble base pair, U13 (red) and Ψ14 (orange) of the U-turn and U10 (yellow) of the U:U base pair. (C) Temperature-dependent 1D-^{1}H imino proton spectra at 10 °C, 25 °C and 40 °C in the absence (left) and presence (right) of 100 mM KCl, respectively.

Supplementary Figure S11.

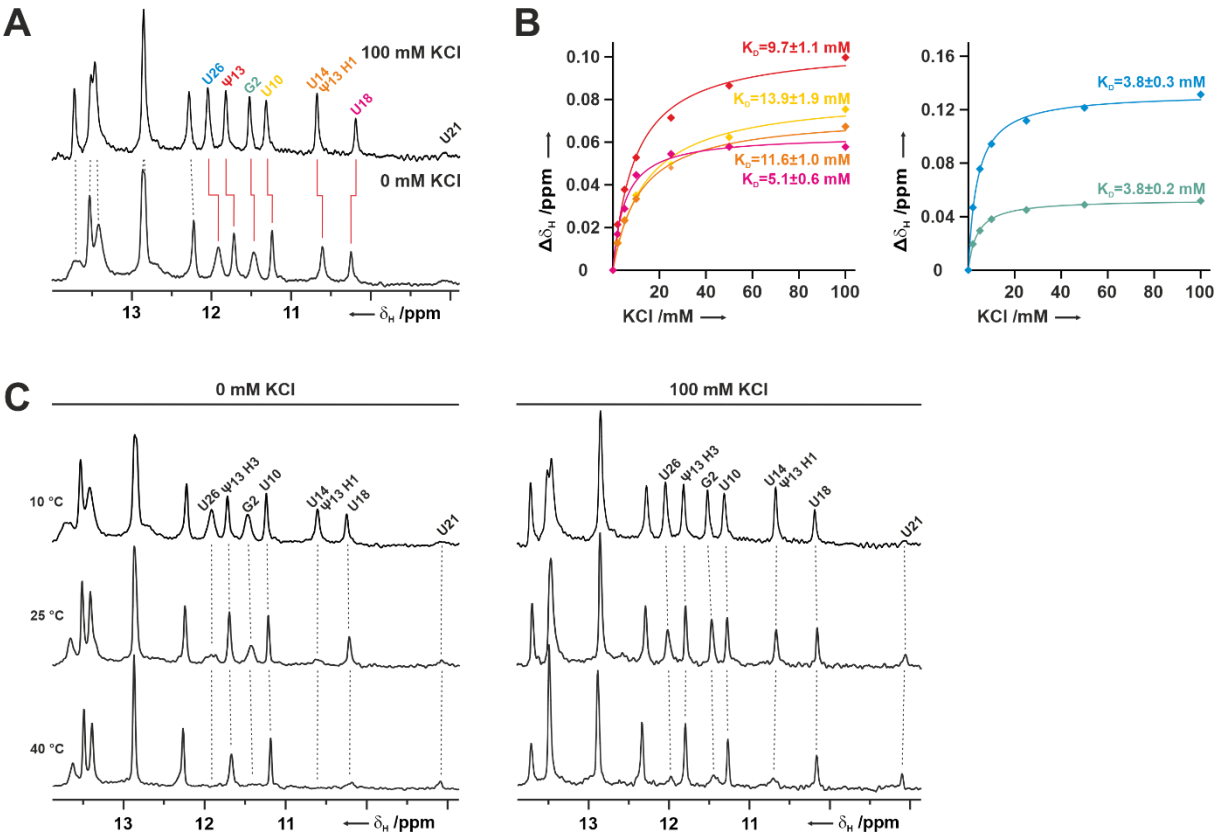

Potassium ion binding to the WT NSR U13Ψ variant. (A) Chemical shift changes of the imino proton resonances induced by the addition of 100 mM potassium chloride to the U13Ψ RNA in 50 mM BisTris buffer. (B) Chemical shift changes as a function of KCl concentration for Ψ13 (red), U14 (orange) and U18 (pink) of the U-turn and U10 (yellow) of the U:U base pair (left) and G2 (light green) and U26 (blue) of the G:U wobble base pair (right). (C) Temperature-dependent 1D-^{1}H imino proton spectra at 10 °C, 25 °C and 40 °C in the absence (left) and presence (right) of 100 mM KCl, respectively.

Supplementary Figure S12.

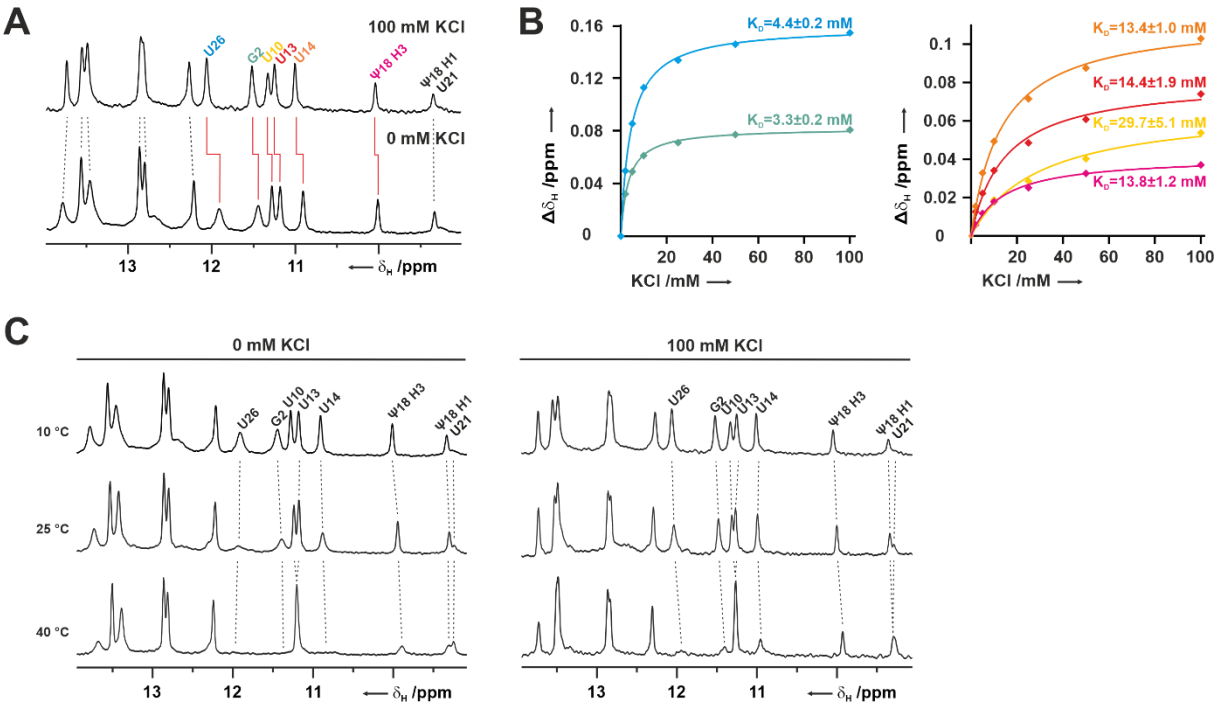

Potassium ion binding to the WT NSR U18Ψ variant. (A) Chemical shift changes of the imino proton resonances induced by the addition of 100 mM potassium chloride to the U18Ψ RNA in 50 mM BisTris buffer. (B) Chemical shift changes as a function of KCl concentration for G2 (light green) and U26 (blue) of the G:U wobble base pair (left) and U13 (red), U14 (orange) and Ψ18 (pink) of the U-turn and U10 (yellow) of the U:U base pair (right). (C) Temperature-dependent 1D-^{1}H imino proton spectra at 10 °C, 25 °C and 40 °C in the absence (left) and presence (right) of 100 mM KCl, respectively.

Supplementary Figure S13.

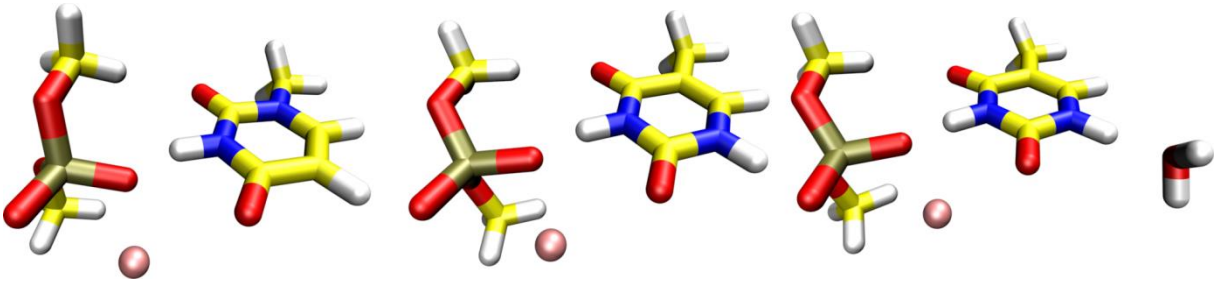

Small model systems representing the HB1 interaction, as seen in the NSR system, which were used in our QM calculations. From left to right, there is an N1-methyl-uracil, a thymine (5-methyl-uracil) as a model compound for pseudouridine, and a thymine with a water bound by the H1N1 imino group, each in a hydrogen-bonded complex with dimethyl phosphate and with a potassium ion present (pink sphere).

Supplementary Figure S14.

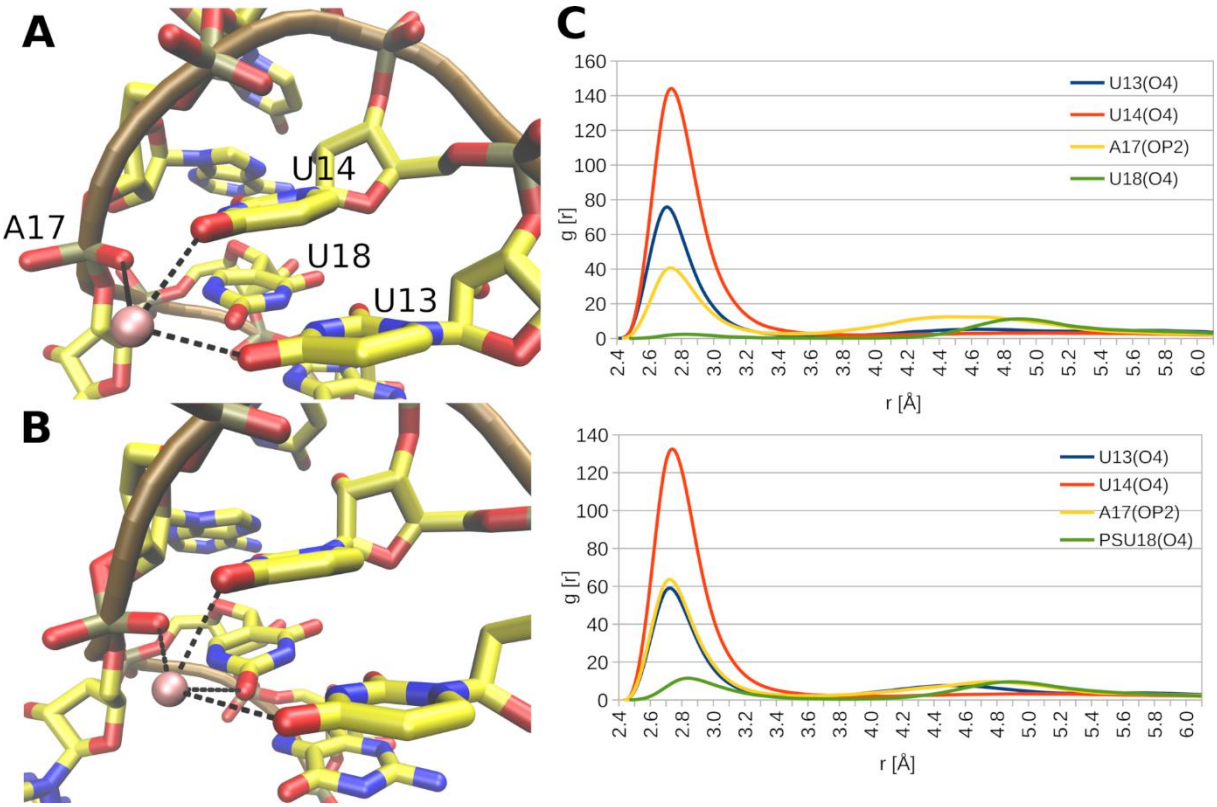

The major (A) and minor (B) potassium ion-binding patterns near the U14 base as observed in MD simulations. The minor binding pattern is significantly populated only in U18Ψ and is characterized by the potassium moving closer to the Ψ18(O2) and A17(OP2) atoms. The RNA coordinating residues are labeled and the ion coordination is indicated by black dashed lines. This ion binding site is completely absent in the $C14^{+}$ variants. (C) Graphs of normalized radial distribution functions for the pair-wise distances (r) between the K^{+} ion and individual coordinating atoms in the unmodified WT NSR (top) and the U18Ψ (bottom) systems.

Supplementary Tables:

Supplementary Table 1.

	$\Delta\delta_H$ [ppm]			$\Delta\delta_P$ [ppm]	$^{2h}J_{HP}$ [Hz]	ΔG_{diss} [kcal/mol]		
	U/Ψ/C14	**U/Ψ13**	**U/Ψ18**	**A17**		**U/Ψ/C14**	**U/Ψ13**	**U/Ψ18**
WT	--	--	--	--	2.82 ± 0.02	3.47 ± 0.04	4.33 ± 0.004	4.30 ± 0.005
U14Ψ	-0.20	+0.02	-0.20	+0.61	2.60 ± 0.04	3.44 ± 0.005	4.01 ± 0.004	3.30 ± 0.001
U13Ψ	-0.05	+0.13	+0.38	+0.01	2.59 ± 0.02	3.11 ± 0.01	5.16 ± 0.02	4.83 ± 0.02
U18Ψ	+0.26	-0.44	+0.22	-0.98	3.03 ± 0.02	4.29 ± 0.02	5.88 ± 0.05	5.14 ± 0.08
U13Ψ_ U18Ψ	+0.23	-0.33	+0.63	-0.99	3.09 ± 0.02	n.d.	n.d.	n.d.
U14C	--	--	--	--	n.d.	2.44 ± 0.03	4.30 ± 0.03	3.95 ± 0.05
U14C_U13Ψ	-0.06	+0.13	+0.40	+0.02	n.d.	2.25 ± 0.02	5.50 ± 0.05	4.97 ± 0.06
U14C_U18Ψ	-0.05	-0.42	+0.18	-0.96	n.d.	2.77 ± 0.02	5.91 ± 0.11	4.96 ± 0.06

- upfield shift
+ downfield shift

Supplementary Table 2.

Geometry parameters of NSR's signature interactions in the MM and QM/MM optimized structures.

	HB1 H-bond distances (in Å) and angles (in °)											
	N3-H3			H3/OP2			N3/OP2			N3/H3/OP2		
method[a]/system	Start	MM	QM/MM	Start	MM	QM/MM	Start	MM	QM/MM	Start	MM	QM/MM
WT	1.013	1.009	1.024	1.95	1.91	1.92	2.95	2.91	2.92	165.46	170.14	166.06
U14Ψ	1.021	1.009	1.023	2.026	1.86	1.91	3.015	2.86	2.91	162.28	170.85	164.46
U14Ψ_2	1.000	1.008	1.018	1.95	1.95	2.09	2.94	2.94	3.10	171.93	167.34	168.48
U18Ψ	0.998	1.012	1.031	1.94	1.82	1.76	2.93	2.82	2.79	168.38	167.65	176.63
	HB2 H-bond distances (in Å) and angles (in °)											
	O2'-HO2'			HO2'/N7			O2'/N7			O2'/HO2'/N7		
WT	0.994	0.981	0.985	1.83	1.81	1.85	2.81	2.79	2.83	173.68	175.09	175.97
U14Ψ	0.962	0.980	0.979	2.01	1.81	1.89	2.97	2.78	2.86	170.83	170.83	175.26
U14Ψ_2	0.983	0.986	0.982	1.68	1.71	1.77	2.66	2.70	2.75	176.05	175.09	174.07
U18Ψ	0.954	0.984	0.990	1.87	1.71	1.67	2.82	2.69	2.66	170.79	173.16	178.26

	U/Ψ14(base)/A16(OP2) anion-π interaction (in Å)		
	Start	MM	QM/MM
WT	2.93	2.97	2.98
U14Ψ	2.99	2.97	2.96
U14Ψ_2	2.87	2.85	2.96
U18Ψ	2.92	2.89	2.85

[a]Method used to perform the optimization: MM – molecular mechanics (OL3); QM – TPSS-D3; QM/MM – TPSS-D3 in the QM part of the system and OL3 in the MM part of the system. All calculations were performed in explicit SPC/E solvent. The U14Ψ system was calculated using two different starting structures.

Pseudouridine library file for MD simulations:

```
!!index array str
 "PSU"
!entry.PSU.unit.atoms table  str name  str type  int typex  int resx  int flags  int seq  int elmnt  dbl chg
 "C5" "CS" 0 1 2293761 1 6 -0.1187
 "C6" "CS" 0 1 2293761 2 6 -0.3291
 "H1" "H4" 0 1 196608 3 1 0.2575
 "N1" "NA" 0 1 2293760 4 7 -0.1450
 "H2" "H" 0 1 196608 5 1 0.2747
 "C2" "C" 0 1 2293761 6 6 0.4973
 "O2" "O" 0 1 196608 7 8 -0.5672
 "N3" "NA" 0 1 2293760 8 7 -0.3024
 "H3" "H" 0 1 196608 9 1 0.2898
 "C4" "C" 0 1 2293760 10 6 0.5585
 "O4" "O" 0 1 196608 11 8 -0.5595
 "P" "P" 0 1 196608 12 15 1.166200
 "OP1" "O2" 0 1 196608 13 8 -0.776000
 "OP2" "O2" 0 1 196608 14 8 -0.776000
 "O5'" "OS" 0 1 196608 15 8 -0.498900
 "C5'" "CI" 0 1 196608 16 6 0.055800
 "H5'" "H1" 0 1 196608 17 1 0.067900
 "H5"" "H1" 0 1 196608 18 1 0.067900
 "C4'" "CT" 0 1 2293760 19 6 0.106500
 "H4'" "H1" 0 1 196608 20 1 0.117400
 "O4'" "OS" 0 1 2293760 21 8 -0.354800
 "C1'" "CT" 0 1 2293760 22 6 0.3180
 "H1'" "H1" 0 1 196608 23 1 -0.0580
 "C2'" "CT" 0 1 2293760 24 6 0.067000
 "H2'" "H1" 0 1 196608 25 1 0.097200
 "O2'" "OH" 0 1 196608 26 8 -0.613900
 "HO2'" "HO" 0 1 196608 27 1 0.418600
 "C3'" "CT" 0 1 2293760 28 6 0.202200
 "H3'" "H1" 0 1 196608 29 1 0.061500
 "O3'" "OS" 0 1 196608 30 8 -0.524600
!entry.PSU.unit.atomspertinfo table  str pname  str ptype  int ptypex  int pelmnt  dbl pchg
 "C5" "CS" 0 -1 0.0
 "C6" "CS" 0 -1 0.0
 "H1" "H4" 0 -1 0.0
 "N1" "N" 0 -1 0.0
 "H2" "H" 0 -1 0.0
 "C3" "C" 0 -1 0.0
 "O1" "O" 0 -1 0.0
 "N2" "N" 0 -1 0.0
 "H3" "H" 0 -1 0.0
 "C4" "C" 0 -1 0.0
 "O2" "O" 0 -1 0.0
 "P" "P" 0 -1 0.0
 "OP1" "O2" 0 -1 0.0
 "OP2" "O2" 0 -1 0.0
```

"O5'" "OS" 0 -1 0.0
"C5'" "CI" 0 -1 0.0
"H5'" "H1" 0 -1 0.0
"H5"" "H1" 0 -1 0.0
"C4'" "CT" 0 -1 0.0
"H4'" "H1" 0 -1 0.0
"O4'" "OS" 0 -1 0.0
"C1'" "CT" 0 -1 0.0
"H1'" "H2" 0 -1 0.0
"C2'" "CT" 0 -1 0.0
"H2'" "H1" 0 -1 0.0
"O2'" "OH" 0 -1 0.0
"HO2'" "HO" 0 -1 0.0
"C3'" "CT" 0 -1 0.0
"H3'" "H1" 0 -1 0.0
"O3'" "OS" 0 -1 0.0
!entry.PSU.unit.boundbox array dbl
-1.000000
0.0
0.0
0.0
0.0
!entry.PSU.unit.childsequence single int
2
!entry.PSU.unit.connect array int
12
30
!entry.PSU.unit.connectivity table int atom1x int atom2x int flags
1 2 1
1 10 1
1 22 1
2 3 1
2 4 1
4 5 1
4 6 1
6 7 1
6 8 1
8 9 1
8 10 1
10 11 1
12 13 1
12 14 1
12 15 1
15 16 1
16 17 1
16 18 1
16 19 1
19 20 1
19 21 1
19 28 1
21 22 1

```
 22 23 1
 22 24 1
 24 25 1
 24 26 1
 24 28 1
 26 27 1
 28 29 1
 28 30 1
!entry.PSU.unit.hierarchy table  str abovetype  int abovex  str belowtype  int belowx
 "U" 0 "R" 1
 "R" 1 "A" 1
 "R" 1 "A" 2
 "R" 1 "A" 3
 "R" 1 "A" 4
 "R" 1 "A" 5
 "R" 1 "A" 6
 "R" 1 "A" 7
 "R" 1 "A" 8
 "R" 1 "A" 9
 "R" 1 "A" 10
 "R" 1 "A" 11
 "R" 1 "A" 12
 "R" 1 "A" 13
 "R" 1 "A" 14
 "R" 1 "A" 15
 "R" 1 "A" 16
 "R" 1 "A" 17
 "R" 1 "A" 18
 "R" 1 "A" 19
 "R" 1 "A" 20
 "R" 1 "A" 21
 "R" 1 "A" 22
 "R" 1 "A" 23
 "R" 1 "A" 24
 "R" 1 "A" 25
 "R" 1 "A" 26
 "R" 1 "A" 27
 "R" 1 "A" 28
 "R" 1 "A" 29
 "R" 1 "A" 30
!entry.PSU.unit.name single str
 "PSU"
!entry.PSU.unit.positions table  dbl x  dbl y  dbl z
 6.291773 3.483933 3.533553
 6.657317 4.188977 4.679021
 6.160227 5.113035 4.934553
 7.647297 3.711838 5.461439
 7.919095 4.221509 6.289664
 8.284492 2.574199 5.154477
 9.187570 2.164650 5.880656
 7.946655 1.881422 4.057235
```

```
 8.443203 1.028593 3.841819
 6.976668 2.294453 3.236002
 6.675163 1.667717 2.222697
 -0.510693 2.314837 2.311008
 -1.094069 2.854583 1.061877
 -0.345128 0.853252 2.473702
 0.923162 3.014033 2.533789
 2.005209 2.705663 1.684707
 2.393793 1.713734 1.916172
 1.655680 2.725350 0.652701
 3.103521 3.752935 1.849116
 2.651254 4.734966 1.988129
 3.955764 3.471812 2.944697
 5.218960 4.005842 2.607315
 5.171158 5.092257 2.677258
 5.392842 3.610871 1.148893
 5.687472 2.563966 1.077897
 6.313133 4.441124 0.476943
 6.362655 4.160940 -0.439978
 3.985940 3.802188 0.602565
 3.723595 3.017345 -0.106803
 3.881125 5.081125 0.018386
!entry.PSU.unit.residueconnect table  int c1x  int c2x  int c3x  int c4x  int c5x  int c6x
 12 30 0 0 0 0
!entry.PSU.unit.residues table  str name  int seq  int childseq  int startatomx  str restype  int
imagingx
 "PSU" 1 31 1 "?" 0
!entry.PSU.unit.residuesPdbSequenceNumber array int
 0
!entry.PSU.unit.solventcap array dbl
 -1.000000
 0.0
 0.0
 0.0
 0.0
!entry.PSU.unit.velocities table  dbl x  dbl y  dbl z
 0.0 0.0 0.0
 0.0 0.0 0.0
 0.0 0.0 0.0
 0.0 0.0 0.0
 0.0 0.0 0.0
 0.0 0.0 0.0
 0.0 0.0 0.0
 0.0 0.0 0.0
 0.0 0.0 0.0
 0.0 0.0 0.0
 0.0 0.0 0.0
 0.0 0.0 0.0
 0.0 0.0 0.0
 0.0 0.0 0.0
 0.0 0.0 0.0
```

0.0 0.0 0.0
0.0 0.0 0.0
0.0 0.0 0.0
0.0 0.0 0.0
0.0 0.0 0.0
0.0 0.0 0.0
0.0 0.0 0.0
0.0 0.0 0.0
0.0 0.0 0.0
0.0 0.0 0.0
0.0 0.0 0.0
0.0 0.0 0.0
0.0 0.0 0.0
0.0 0.0 0.0
0.0 0.0 0.0

Pseudouridine parameter file for MD simulations:

```
#   Modifications for PSU
BOND
CS - NA   500.0   1.3400

ANGLE
CS - CS - CT 70.0    118.50
CS - CS - NA 70.0    122.01
CS - NA - H  50.0    118.17
CS - NA - C  70.0    123.66
H4 - CS - NA 50.0    118.99
NA - C - NA  70.0    114.38

DIHE
X-CS-NA-X     2    7.50          180        2.0
X-CT-NA-X     6    0.00           0         2.0
OS-CT-CS-CS   1    1.02514     149.8583       -1.      ol3 chi ura - adapted for PSU
OS-CT-CS-CS   1    1.74876      16.7648       -2.      ol3 chi ura - adapted for PSU
OS-CT-CS-CS   1    0.58150     179.3474       -3.      ol3 chi ura - adapted for PSU
OS-CT-CS-CS   1    0.35148      16.0016        4.      ol3 chi ura - adapted for PSU
```

References

Ahlrichs R, Bär M, Häser M, Horn H, Kölmel C. 1989. Electronic structure calculations on workstation computers: The program system turbomole. *Chem Phys Lett* **162**: 165–169. doi: 10.1016/0009-2614(89)85118-8

Brandenburg JG, Hochheim M, Bredow T, Grimme S. 2014. Low-cost quantum chemical methods for noncovalent interactions. *J Phys Chem Lett* **5**: 4275–4284. doi: 10.1021/jz5021313

Götz AW, Clark MA, Walker RC. 2014. An extensible interface for QM/MM molecular dynamics simulations with AMBER. *J Comput Chem* **35**: 95–108. doi: 10.1002/jcc.23444

Grimme S, Brandenburg JG, Bannwarth C, Hansen A. 2015. Consistent structures and interactions by density functional theory with small atomic orbital basis sets. *J Chem Phys* **143**: 54107. doi: 10.1063/1.4927476

Krepl M, Vögele J, Kruse H, Duchardt-Ferner E, Wöhnert J, Sponer J. 2018. An intricate balance of hydrogen bonding, ion atmosphere and dynamics facilitates a seamless uracil to cytosine substitution in the U-turn of the neomycin-sensing riboswitch. *Nucleic Acids Res* **46**: 6528–6543. doi: 10.1093/nar/gky490

Pokorná P, Kruse H, Krepl M, Šponer J. 2018. QM/MM calculations on protein-RNA complexes: understanding limitations of classical MD simulations and search for reliable cost-effective QM methods. *J Chem Theory Comput* **14**: 5419–5433. doi: 10.1021/acs.jctc.8b00670